Ventom, A. M., Deistung, J., & Bray, R. C. (1988) *Biochem. J. 255*, 949–956.
Vogel, H. J. (1984) in *Phosphorus-31 NMR: Principles and Applications* (Gorenstein, D. G., Ed.) pp 105–154, Academic Press, New York.
Wootton, J. C., Nicolson, R. E., Cock, J. R., Walters, D. E., Burke, J., Doyle, W., & Bray, R. C. (1991) *Biochim. Biophys. Acta* (in press).

Ligand Binding and Protein Relaxation in Heme Proteins: A Room Temperature Analysis of NO Geminate Recombination†

J. W. Petrich,‡,§ J.-C. Lambry,‡ K. Kuczera,∥ M. Karplus,*,∥ C. Poyart,⊥ and J.-L. Martin*,‡
Laboratoire d'Optique Appliquée, Ecole Polytechnique, ENSTA, INSERM U275, 91128 Palaiseau Cedex, France, Department of Chemistry, Harvard University, Cambridge, Massachusetts 02138, and INSERM U299, 94275 Le Kremlin-Bicêtre, France
Received July 10, 1990; Revised Manuscript Received November 1, 1990

ABSTRACT: Ultrafast absorption spectroscopy is used to study heme–NO recombination at room temperature in aqueous buffer on time scales where the ligand cannot leave its cage environment. While a single barrier is observed for the cage recombination of NO with heme in the absence of globin, recombination in hemoglobin and myoglobin is nonexponential. Examination of hemoglobin with and without inositol hexaphosphate points to proximal constraints as important determinants of the geminate rebinding kinetics. Molecular dynamics simulations of myoglobin and heme–imidazole subsequent to ligand dissociation were used to investigate the transient behavior of the Fe–proximal histidine coordinate and its possible involvement in geminate recombination. The calculations, in the context of the absorption measurements, are used to formulate a distinction between nonexponential rebinding that results from multiple protein conformations (substates) present at equilibrium or from nonequilibrium relaxation of the protein triggered by a perturbation such as ligand dissociation. The importance of these two processes is expected to depend on the time scale of rebinding relative to equilibrium fluctuations and nonequilibrium relaxation. Since NO rebinding occurs on the picosecond time scale of the calculated myoglobin relaxation, a time-dependent barrier is likely to be an important factor in the observed nonexponential kinetics. The general implications of the present results for ligand binding in heme proteins and its time and temperature dependence are discussed. It appears likely that, at low temperatures, inhomogeneous protein populations play an important role and that as the temperature is raised, relaxation effects become significant as well.

The microscopic aspects of ligand binding in myoglobin and hemoglobin are not fully understood, although great progress has been made recently in their analysis. Structural disorder and its temporal evolution (Frauenfelder et al., 1979; Case & Karplus, 1979; Debrunner & Frauenfelder, 1982; Elber & Karplus, 1987a,b) apparently play an important role. The high-resolution X-ray structures of ligated and unligated myoglobin do not reveal any path by which ligands can move between the heme binding site and the outside of the protein (Perutz & Mathews, 1966; Takano, 1977). Since motion must therefore be involved in the ligand binding, myoglobin has become a model system for studying the relation of motion to function in proteins.

Much of what is known about the influence of protein fluctuations on heme protein reactivity is due to measurements of ligand recombination after photodissociation on the nanosecond to second time scales. A series of studies (Austin et al., 1975; Henry et al., 1983; Ansari et al., 1985) have suggested that a phenomenological description of the kinetics of photodissociation and rebinding of a ligand X to myoglobin (Mb) can be written as

$$\mathrm{MbX} \rightleftarrows (\mathrm{Mb} + \mathrm{X})_{\mathrm{pocket}} \rightleftarrows (\mathrm{MB} + \mathrm{X})_{\mathrm{protein}} \rightleftarrows (\mathrm{Mb} + \mathrm{X})_{\mathrm{solution}}$$

where the subscript refers to the location of the ligand X. Each of the designated species may involve several different states or substates on a microscopic level. At low temperatures (below 200 K in ethylene glycol/water), it is found that the geminate rebinding of the CO ligand is nonexponential. This has been attributed to a distribution of barrier heights, associated with the different substates that equilibrate slowly relative to the rebinding. As the temperature is raised, the geminate recombination of CO becomes exponential and can be described by a single barrier.

In analyzing the origin of the nonexponential behavior and, more generally, the complexity of the rebinding kinetics in proteins, it is important to consider two types of motional phenomena (Ansari et al., 1985). One of these consists of the fluctuations that occur at equilibrium. These equilibrium fluctuations consist of motions within a potential well at low temperature. At higher temperatures transitions between wells are superposed on the harmonic fluctuations (Elber & Karplus, 1987; Smith et al., 1990). The other type of motion arises in a nonequilibrium system and corresponds to relaxation toward equilibrium. Since photodissociation creates a nonequilibrium

† During the course of this work, J.W.P. was the recipient of an NSF Industrialized Countries postdoctoral fellowship, an INSERM *poste orange*, and fellowships from La Fondation pour la Recherche Médicale and the Ecole Polytechnique. Parts of this work were funded by INSERM, ENSTA, le Ministre de la Recherche et de la Technologie, the National Science Foundation, and the National Institutes of Health.
‡ INSERM U275.
§ Present address: Department of Chemistry, Iowa State University, Ames, IA 50011.
∥ Harvard University.
⊥ INSERM U299.

0006-2960/91/0430-3975$02.50/0

state of the heme protein (i.e., an unligated heme with the iron in the plane), both equilibrium-type fluctuations and relaxation can be present during the ligand rebinding process which is being studied experimentally. Nonexponential rebinding can arise, as already mentioned, from a distribution of barriers associated with different protein molecules (an inhomogeneous population) that is present when the transitions between substates are slow relative to the rebinding rate. An alternative possibility that has been considered and excluded experimentally is that the complex rebinding behavior arises from a homogeneous population with multiple binding sites (Austin et al., 1975). Nonexponential behavior can also arise from protein relaxation on the time scale of the rebinding process if the barrier height is a function of time. The barrier to rebinding is expected to be lowest when the iron is in the heme plane and to increase as the heme moves out of the plane and the protein relaxes to the unligated equilibrium structure.

Frauenfelder and co-workers have done multiflash experiments on MbCO (Austin et al., 1975) to determine whether the low-temperature nonexponential behavior arises from an inhomogeneous protein population or from a homogeneous population with multiple binding sites. They concluded that only the former was in accord with the experiments because the observed rebinding behavior was the same for consecutive flashes, though in subsequent more detailed experiments a small amount of "pumping", suggesting multiple sites, was observed (Ansari et al., 1987). They did not consider explicitly the possibility of relaxation in interpreting the multiflash experiment. If nonexponential behavior arises from the time-dependent relaxation of a homogeneous protein population and the intervals between flashes are long enough for the ligated protein to be fully relaxed when the next flash occurs, the same rebinding behavior is expected for each flash. Thus, time-dependent relaxation, as well as an inhomogeneous protein population with different barriers, could contribute to the observed behavior.

In myoglobin, at low temperatures (below about 160 K), the very long times over which the CO rebinding is nonexponential and some of the long time delay flash experiments demonstrate that an inhomogeneous model is required (Ansari et al., 1987). At room temperature, where CO rebinding is exponential, the observed time scale for rebinding ($\sim$100 ns) (Henry et al., 1983) is slower than the time for protein relaxation ($\sim$2–100 ps) found in the present simulations. However, as has been suggested by Agmon and Hopfield (1983), it is likely that protein relaxation plays a role in the rebinding kinetics in the intermediate temperature range. Because of the much lower barrier for rebinding of NO versus CO, 80% of the NO molecules have rebound within 300 ps at room temperature. Thus protein relaxation to equilibrium after photodissociation is likely to occur on the same time scale as the rebinding. Since NO binding is, in fact, nonexponential at room temperature, it is useful for studying the nature of the rebinding process under physiological conditions.

The above discussion raises a number of questions. Are different protein configurations involved in ligand rebinding at room temperature; and if so, on what time scale do they interconvert? More generally, do distributions of protein configurations play a role in the kinetics of the biologically important processes that take place at room temperature? Are the configurations of the protein that govern the rate of rebinding localized, or are they coupled to parts of the protein far removed from the binding site? (Most available measurements are sensitive only to regions near the heme.) Can nonexponential rebinding kinetics arise from relaxation of a reactive coordinate triggered by ligand dissociation? We address these questions by using femtosecond absorption spectroscopy and molecular dynamics simulations to study ligand rebinding in heme proteins at room temperature.

The barrier to ligand rebinding is a combination of electronic (Chernoff et al., 1980; Cornelius et al., 1983; Petrich et al., 1988a) and steric factors (Szabo, 1978; Case & Karplus, 1979; Frauenfelder & Wolynes, 1985). The rebinding of NO is very rapid because the barrier is greatly diminished with respect to that of other ligands, such as O_2 and CO. Thus, the study of NO permits a more direct investigation of the transient structural factors affecting ligand rebinding at room temperature. Further, it has been shown that NO rebinding is not sensitive to ligand concentration on the several hundred picosecond time scale (Martin et al., 1983), which implies that geminate or cage recombination is involved. To aid in the interpretation of the experimental studies of the ligand rebinding kinetics, comparisons were made with the results of molecular dynamics simulations of the dissociation of carbon monoxide from a model heme compound, heme–imidazole (HI), and from myoglobin. Since the focus of the simulations is the protein response to the perturbation caused by ligand dissociation, rather than the specific interactions of the ligand and the heme, the use of CO as a ligand, rather than NO, should not present a problem. Of particular interest is the displacement of the Fe from the heme plane after photodissociation and the coupling of the displacement to relaxation of the protein.

Materials and Methods

In this section we outline the experimental and theoretical procedures. Only a brief discription is given with emphasis on the aspects most relevant to the present studies; details are given in some of the references.

(*A*) *Measurement of Geminate Recombination Kinetics.* Ultrafast absorption measurements were performed at the Laboratoire d'Optique Appliquée. The apparatus used to obtain the recombination kinetics and the preparation of the samples are described in detail elsewhere (Petrich et al., 1988a). The following systems were studied: protoheme (PTH); sperm whale myoglobin (Mb); hemoglobin (Hb), with and without inositol hexaphosphate (IHP); and the symmetrical valency hybrid hemoglobins, $\alpha_2^{NO}\beta_2^{+CN}$ and $\alpha_2^{+CN}\beta_2^{NO}$, with and without IHP. As was shown in Petrich et al. (1988a), NO is photodissociated from the heme in less than 50 fs. The time course of the rebinding is followed by monitoring the transmission, $I(t)/I_0$, of a weak, tunable probe beam through the sample. The probe transmission is determined with a photodiode and normalized with respect to a reference beam. Using photodiodes to detect the transient absorbance changes is preferable to alternative methods employing vidicons (Jongeward et al., 1986, 1988). Diodes provide a much larger linear response and do not produce the base-line fluctuations that are typical of vidicons (Petrich et al., 1988a; Janes et al., 1988). The measured values of $I(t)/I_0$ are converted to the sample absorbance changes, $\Delta A(t)$, which in turn are equal to the normalized number of unligated hemes, $N(t)$, where $N(0)$ is set equal to unity.

We use several different functions to analyze the data so as to be able to obtain information on the origin of deviations from single-exponential rebinding kinetics. The functions are

$$\Delta A(t) = \exp(-t/\tau) + \text{constant} \quad (1)$$

$$\Delta A(t) = A \exp(-t/\tau_1) + (1 - A) \exp(-t/\tau_2) \quad (2)$$

$$\Delta A(t) = (1 + t/\tau_0)^{-n} \quad (3)$$

$$\Delta A(t) = \exp\left[-\int_0^t k(t)\,dt\right] \quad (4)$$

The data are fit to each functional form by a least-squares procedure utilizing the Marquardt algorithm (Bevington, 1969). In addition, geminate ligand binding has been described by diffusion-controlled models (Agmon, 1985; Marden et al., 1986) and by the Kohlrausch relaxation function, $f(t) = \exp[-(t/\tau)^\alpha]$, which has been used also for nonexponential relaxation processes in glasses (Plonka, 1988). The latter two models are not considered here.

A recombination process fitted by a single or a double exponential (eq 1 and 2) is often interpreted as arising from one or two physical barriers, respectively. However, such a fit does not demonstrate that such a simple interpretation is correct. Also, eq 1 for a nonzero base line is a special case of the double exponential (eq 2), where the second recovery time is long on the time scale of the measurement. In the presence of a "base line", the simple interpretation of single-exponential geminate binding is warranted only if the slowly recovering component corresponds to a process other than geminate recombination (e.g., bimolecular recombination after ligand escape from the heme pocket). Escape from the heme pocket and a slow bimolecular rebinding process may be what is observed in the recombination of NO with *Aplysia punctata* myoglobin (Petrich et al., 1988b); Mb from *Aplysia* is unusual in that it lacks the distal histidine (Tentori et al., 1971). In PTHNO the escape of NO from the geminate heme is also likely to be the long-lived process observed (Figure 3A). It is not expected to be the case for sperm whale myoglobin or human hemoglobin studied here, in disagreement with the tacit assumption made by Jongeward et al. (1986, 1988) in their analysis of myoglobin.

The use of a power law (eq 3) was proposed by Austin et al. (1975). They suggested that the rebinding was determined by a distribution, $g(E)$, of barriers so that the number of unligated Mb hemes as a function of time is given by the expression

$$N(t) = \int_0^\infty dE\, g(E) \exp(-kt) \quad (5)$$

where k is the rate constant for a barrier of energy E, corresponding to the Arrhenius equation

$$k = A \exp(-E/RT) \quad (6)$$

Here R is the molecular gas constant and T is the absolute temperature. The problem is to analyze the data to determine the distribution of activation barriers, $g(E)$ [or, more precisely, $g[E(k)]$]. An analytical solution for $g[E(k)]$ can be obtained by changing the variable of integration from E to k and assuming that the limits of integration remain the same, i.e.

$$N(t) = \int_0^\infty dk\, (RT[g[E(k)]/k]) \exp(-kt) \quad (7)$$

The form of $g[E(k)]$ was obtained by Austin et al. (1975), by noting that the low-temperature Mb data could be adequately described by eq 3. Since $g[E(k)]$ is related to the power law expression by the Laplace transform defined in eq 7, it follows that

$$g[E(k)] = (\tau_0 k)^n e^{-\tau_0 k}/[\Gamma(n)RT] \quad (8)$$

where $\Gamma(n)$ is the gamma function, and the peak of the distribution occurs at $k^{peak} = n/\tau_0$.

Equation 4 corresponds to the possibility that the nonexponential behavior can be produced by a time-dependent evolution of the barrier for the rebinding process. The disappearance of unligated protein, $N(t)$, follows the modified first order decay law

$$-dN/dt = k(t)N \quad (9)$$

Integration of this expression gives $N(t) = N_0 \exp[-\int_0^t k(t)\,dt]$, from which we obtain eq 4. A simple form of $k(t)$ is obtained from the modified Arrhenius equation

$$k(t) = A \exp[-E(t)/RT] \quad (10)$$

with

$$E(t) = (E_0 - E_{eq}) \exp(-k_{bar}t) + E_{eq} \quad (11)$$

where k_{bar} is the rate constant that determines the decay of the initial barrier height, E_0, to its equilibrium value, E_{eq}. In general, for a complex system (Bay & Fayer, 1989) such as a protein, $E(t)$ may consist of a sum of terms involving relaxation processes on different time scales or be represented by a power law, analogous to eq 3.

Because this study is concerned with the geminate recombination processes that occur on the picosecond time scale, the effect of convolution of the 100–150-fs laser pulse is negligible and has not been included in the fitting procedure. For the same reason, the 300-fs rise time of the deligated species (Martin et al., 1983; Petrich et al., 1988a) has not been included in the description of the kinetics. As has been discussed in detail elsewhere (Petrich et al., 1988a), we take the quantum yield of NO photodissociation to be unity for all the systems studied. The absorption changes are normalized such that the absorption change at time zero is one. The maximum absorption change, ΔA_{max} at $t = 0$, is given for each species in the figure captions. The wavelengths at which the geminate recombination is monitored (see the appropriate figures and their captions) correspond to the maximum or near the maximum of the Soret band of the equilibrium unligated species. Previous studies have indicated that the time evolution of the spectra of the excited-state species of heme proteins bound to various ligands does not contribute to the recombination kinetics measured here because they are considerably red shifted and very short lived (300 fs and 2.5 ps).

The analysis of the paper assumes that the observed spectral changes measure ligand rebinding. If the observed spectral changes in the region of interest were due (to a significant extent) to conformational changes, such changes should be clearly seen in photolyzed CO-ligated heme proteins. At the wavelengths we are probing in the present study, the contribution of the 2.5-ps excited state is negligible and the only time evolution arises from the 300-fs component (the time constant of the appearance of the deoxy species). In photodissociated MbCO, other than the 300-fs component, there is no detectable kinetic evolution up to 500 ps, in accord with the fact that the CO rebinding process is occurring on the nanosecond time scale. The Soret band difference spectrum remains stationary up to 6.5 ns (Janes et al., 1988). In photodissociated Hb, the picosecond spectrum is slightly different from that observed at steady state. The presence of a slowly evolving (nanosecond to millisecond) distortion of the transient spectrum has been attributed (Hofrichter et al., 1983; Petrich et al., 1988) to the time evolution of the constraints present in the cooperative tetramer. On the time scale of the present study, this relaxation component is negligible and does not affect the measured kinetics.

(*B*) *Theoretical Methodology*. The methodology used for the molecular dynamics simulation of the photodissociation corresponds to that employed previously in studies of the equilibrium structure and fluctuations of MbCO as a function of temperature (Kuczera et al., 1990). These simulations yielded results for the temperature dependence of the structure and mean fluctuations in agreement with X-ray and incoherent

Table I: Potential Energy Parameters That Differ for the Ligated (HICO, MbCO) and Unligated (HI + CO, Mb + CO) Systems[a]

		ligated[b]		unligated[c]	
		force constant	equilibrium value	force constant	equilibrium value
		Bonds			
(Mb)	Fe–Np	540	1.958	540	2.1
(HI)	Fe–NE2	130	2.2	130	2.1
		Angles			
(Mb)	Np–Fe–Np	28.8	90	160	90
(HI)	NE2–Fe–Np	100	90	100	107

[a] Bond lengths in Å, angles in deg; the corresponding force constants are in kcal/(mol·Å^2) and kcal/(mol·rad^2), respectively. Np = heme pyrrole nitrogen, NE2 = nitrogen of His linked to Fe. [b] From Kuczera et al. (1990). [c] From Y. Arata and M. Karplus (unpublished results); the geometric parameters were obtained from Perutz et al. (1987).

neutron scattering results (Smith et al., 1990). The potential energy function used to represent the system contained harmonic terms corresponding to bond stretching, angle bending, and improper dihedral angle deformations, a cosine term for dihedral angles, and Lennard-Jones and electrostatic terms for nonbonded interactions. All polar hydrogen atoms were explicitly included in the calculations, while those appearing in aliphatic and aromatic nonpolar groups were treated by the extended atom approximation. The MbCO system thus consists of 1536 atom (1217 protein heavy atoms, 270 protein polar hydrogens, 43 heme heavy atoms, 4 heme meso hydrogens, and 1 CO molecule); the HICO system consisted of 55 atoms (5 imidazole heavy atoms, 1 imidazole polar hydrogen, and heme and CO as for MbCO). No special terms were employed for hydrogen bonds. A nonbonded interaction cutoff distance of 7.5 Å was used together with a 1-Å switching function to eliminate discontinuities due to the cutoff. A distance-dependent dielectric function ($\epsilon = r$) was employed (Brooks et al., 1983). The potential energy parameters for the ligated systems were the same as used in previous MbCO simulations (Kuczera et al., 1990). Those for the unligated hemes were obtained from an analysis of structural and vibrational properties of five-coordinate hemes (Y. Arata and M. Karplus, unpublished results); the parameter values are presented in Table I.

The molecular dynamics simulations were done with the Verlet algorithm and an integration step size of 0.001 ps. Bonds involving hydrogen atoms were kept fixed with the SHAKE algorithm (van Gunsteren & Berendsen, 1977). Simulations were performed with the program CHARMM (Version 21) (Brooks et al., 1983) on a CRAY-XMP computer at the Naval Research Laboratories at Arlington, VA. The analyses of the trajectories were made on VAX 11/780 and CONVEX computers at Harvard University.

Molecular dynamics simulations of photodissociation were performed for the model system heme–imidazole–CO (HICO) and (carbonmonoxy)myoglobin (MbCO); we use the notation HICO to distinguish the simulation system that includes an axial histidine from the heme–NO (PTH NO) used in the experiments. Preliminary trajectories of 70 ps for HICO at 300 K and 200 ps for MbCO at 325 K were performed. From these trajectories, certain coordinate sets and the associated velocities were chosen as starting points for the dissociation simulation; six sets (at 40, 45, 50, 55, 60, and 65 ps) were used for HICO and three (at 50, 60, and 80 ps) for MbCO.

To generate the transition from the ligated to the unligated state, a simple approximation to the behavior of the heme group after photoexcitation was introduced. Light absorption brings the ligated heme to an excited dissociative electronic state, which then decays to the ground electronic state of the unligated heme. These processes are very fast. There is evidence that the Fe–C bond is broken in less than 50 fs, while an electronic absorption spectrum very similar to that of the equilibrium unligated species appears in about 300 fs (Martin et al., 1983; Petrich et al., 1988a). In the simulations, the sudden approximation was used to generate the transition of the heme from the ligated to the excited unligated species. A 0.2-ps trajectory was calculated, with the initial conditions corresponding to the selected coordinate sets described above. Geometric and energetic parameters for a five-coordinate domed heme group corresponding to unligated Mb were introduced, and a special potential energy function for the interaction between the heme and the CO molecule was used. The Fe···C interaction was represented by r^{-12} repulsion, with an energy of 10 kcal/mol for the distance corresponding to the initial coordinate set; all other heme–CO interactions were set to zero. The Fe···C repulsion mimics the motion of the CO molecules on the repulsive energy hypersurface of the dissociative excited state (Korzekwa et al., 1985). For a set of points along the 0.2-ps trajectory (every 5 fs), energies were calculated for both the special repulsive potential and the unligated heme potential with the full heme–CO nonbonded interactions. A series of times were determined for which the calculated energy difference between the modified and standard potentials was no larger than 0.2 kcal/mol. (The total potential energy was about −2000 kcal/mol for MbCO and 100 kcal/mol for HICO.) Matching values of the energy were found for times in the range from 100 to 150 fs. A particular value in this range was chosen as t_0, and the simulation was restarted at that point with the standard unligated potential energy function and continued for the desired simulation period. Thus, the system makes a transition to the ground-state unligated potential energy surface at time t_0. To describe this state, standard interactions between the unligated heme protein and the CO are used, but no Fe–CO bonding interaction is included. The latter eliminates the possibility of rebinding for the CO since the present simulations are made to study protein relaxation after photodissociation and not rebinding.

Given the initial coordinates and velocities for the dissociated system, six trajectories 5 ps in length were calculated for HI and three trajectories (each 100 ps in length) were calculated for Mb. The average temperatures were near 300 K.

RESULTS

(A) Molecular Dynamics Simulations

(i) Dissociation Dynamics of the Heme–Imidazole–CO (HICO) Model System. To have a basis for determining the effects of the protein on the dissociation dynamics of MbCO, the model system HICO was studied. For both HICO and HI the structural heme geometries obtained from energy minimization and the molecular dynamics averages are very similar (see Table II). For HICO, the heme is essentially planar with the Fe atom 0.02 Å or less from the heme plane. In HI, the heme group is domed with the Fe atom 0.48 Å from the mean plane of the four pyrrole nitrogens (plane 1) and 0.68 Å from the mean plane of the 24 porphyrin heavy atoms (plane 2). These values for HICO and HI are in the range of the iron out-of-plane displacements and doming found for ligated and unligated model porphyrins, myoglobins, and hemoglobin; that is, the Fe–heme distance is essentially zero and the overall heme geometry is nearly planar for six-coordinated systems, while for a five-coordinated heme the Fe distance from plane 1 is 0.3–0.4 Å and from plane 2 is 0.4–0.6 Å with the heme

Table II: Fe Out-of-Plane Displacements for HICO and HI[a]

	ligated	unligated
Energy-Minimized Structures		
Fe–plane 1	0.02	0.47
Fe–plane 2	0.01	0.68
Molecular Dynamics Averages		
Fe–plane 1	0.01	0.48
Fe–plane 2	0.01	0.69

[a] Energy minimizations are for heme–imidazole–CO (HICO) and for heme–imidazole (HI); molecular dynamics are for HICO and the HI + CO system. Plane 1 is the plane of the 4 heme pyrrole nitrogens; plane 2 is the mean plane of the 24 heavy atoms of the heme porphyrin core. The dynamics averages are over a 70-ps trajectory for HICO and over six 5-ps trajectories with different initial conditions for HI + CO. All distances are in Å.

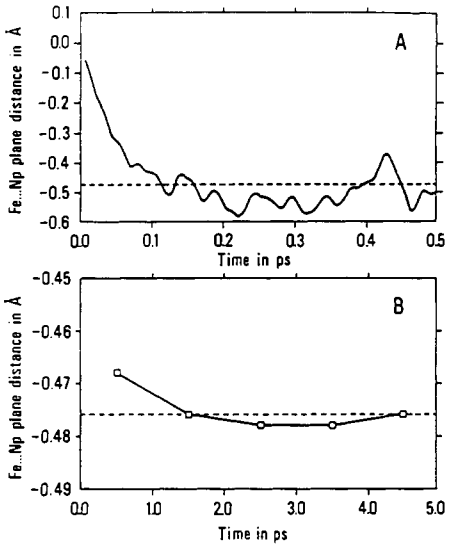

FIGURE 1: Time evolution of the displacement of the Fe atom from the mean plane of the four heme pyrrole nitrogens (Np; plane 1) for HI + CO. Results shown are for the HI + CO trajectory started at t = 70 ps from the HICO simulation (see text). (A) Evolution during the first 0.5 ps. (B) Averages over consecutive 1-ps blocks between 0 and 5 ps; the left-hand-most square corresponds to 0–1 ps, the second to 1–2 ps, and so on. The dashed line corresponds to the average value over the final 4 ps.

domed and/or ruffled (Perutz et al., 1987).

For the six 5-ps HICO dissociation simulations, the initial total energy of the system increased by 41–56 kcal/mol (average of 44 kcal/mol) as a result of the change of parameters corresponding to the photodissociation process. In flash photolysis experiments, typical wavelengths of the photon used for dissociation are 353–585 nm. The energy of a 585-nm photon is 49 kcal/mol, and the energy of a 353-nm photon is 81 kcal/mol. Since the Fe–C bond dissociation energy is about 22 kcal/mol (Keyes et al., 1971), an excess photon energy of 27–59 kcal/mol is available, which is in accord with the simulation values. There is no experimental result concerning the inital energy distribution. In the simulation, the energy is initially localized in the broken Fe···CO bond and in the Fe···porphyrin linkage. Because an isolated system is being studied (microcanonical ensemble), the excess energy remains in the HI + CO system during the simulation.

The iron atom out-of-plane motion in the dissociation simulations consisted of a fast initial relaxation, followed by oscillations around an equilibrium value (see Figure 1). The time constant of the initial relaxation in the six 5-ps trajectories varied between 30 and 70 fs, with an average value of 51 fs. After 1 ps, the average geometry of the heme was very close to that of the energy-minimized unligated system. These

Table III: Geometries of the Heme and Heme–Histidine Linkage of Ligated and Unligated Myoglobin

	ligated Mb			unligated Mb		
	MbCO[a]	MbO_2[b]	MD[c]	Mb[d]	Mb[e]	MD[f]
Distances (Å)						
Fe–NA[g]	2.00	1.99	1.96	2.07	2.00	2.07
Fe–NB	1.90	1.90	1.96	2.06	1.97	2.07
Fe–NC	1.91	1.99	1.96	2.06	2.03	2.07
Fe–ND	2.00	2.00	1.95	2.06	2.09	2.07
Fe–NE2	2.06	2.19	2.21	2.12	2.10	2.02
CE1–NA	3.32	3.10	3.09	3.50	3.20	3.25
CD2–NC	3.20	3.07	3.09	3.44	3.46	3.34
Fe–plane 1	0.18	0.00	0.00	0.42	0.30	0.42
Fe–plane 2	0.19	0.03	0.00	0.50	0.35	0.56
Bond Angles (deg)						
CE1–NE2–Fe	130	130	127	128	130	126
CD2–NE2–Fe	121	119	122	122	120	122
NE2–Fe–NA	103	87	90	102	100	99
NE2–Fe–NB	91	91	89	92	96	101
NE2–Fe–NC	94	93	91	102	100	104
NE2–Fe–ND	94	89	89	111	100	101
Dihedral Angles						
CD2–NE2–Fe–NC	2	−4	−1	24	2	−2

[a] X-ray structure of MbCO; Kuriyan et al. (1986). [b] X-ray structure of MbO_2; Phillips (1980). [c] 50–150-ps average structure of MbCO from this work and Kuczera et al. (1990). [d] X-ray structure of Mb; Takano (1977). [e] X-ray structure of Mb; Phillips (1980). [f] 100-ps average structure of Mb from one Mb + CO simulation; this work. [g] NA, NB, NC, and ND labels the four Np nitrogens according to the convention of Perutz et al. (1987).

results are similar to those obtained in a previous simulation of protoheme–CO photodissociation (with a somewhat different empirical potential) by Henry et al. (1985). They observed an initial Fe out-of-plane displacement in 50–150 fs and complete heme relaxation after 1 ps.

The results obtained for HICO and HI + CO are also in general agreement with experimental data on protoheme–CO dissociation dynamics; i.e., the estimated time constant for out-of-plane motion is about 50 fs, and the transient absorption spectrum becomes identical with the equilibrium spectrum within 8 ps after dissociation (Petrich et al., 1988a). The relative contributions of structural relaxation and vibrational cooling to the behavior of the optical spectrum over the 8-ps time period are not known. A solution simulation of HICO dissociation is in progress to examine this question in more detail.

(ii) Dissociation Dynamics of (Carbonmonoxy)myoglobin (MbCO). The 100-ps trajectory average structures of the heme linkage before and after dissociation for the first trajectory are given in Table III. The values of the calculated bond lengths, bond angles, and dihedral angles for the heme are very close to the X-ray crystallographic results for MbCO (Kuriyan et al., 1986), MbO_2 (Phillips, 1980), and deoxy-Mb (Takano, 1977; Phillips, 1981). In the unligated Mb, the Fe–NE2 bond distance, however, is somewhat smaller (by 0.04–0.08 Å) than the corresponding equilibrium value (see Table I) and the Fe atom out-of-plane displacement relative to plane 1 in the Mb + CO simulation is smaller (by 0.05–0.1 Å) than that found for the model system HI + CO (Table II); the ranges indicated arise from the three simulations. Corresponding results are obtained for the average over the final 5 ps of the Mb simulation. Thus, the Fe–heme mean plane (plane 2) distance is between 0.1 and 0.2 Å less in Mb + CO than in HI + CO, indicating that the presence of the protein environment inhibits the relaxation of the heme conformation in Mb after ligand dissociation. Experimentally, the Mb and HI values are very

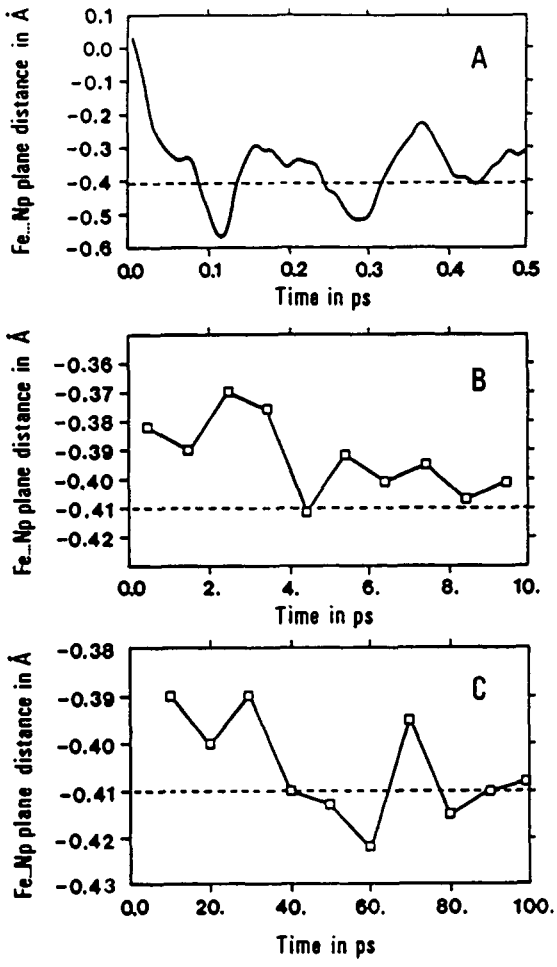

FIGURE 2: Time evolution of the displacement of the Fe atom from the mean plane of the four heme pyrrole nitrogens (Np; plane 1) for Mb + CO. (A) Evolution during the first 0.5 ps. (B) Evolution during the first 10 ps, averages over consecutive 1-ps blocks; the left-hand-most square corresponds to 0–1 ps and so on. (C) Evolution over 100 ps; averages over consecutive 10-ps blocks; the left-hand-most square corresponds to 0–10 ps and so on. The dashed line corresponds to the average value over the final 30 ps.

similar. More important, since the same parameters are used for simulation of Mb and HI, the calculated difference indicates that complete relaxation has not taken place in Mb + CO over the 100 ps of the simulation; by contrast, the HI relaxation is essentially complete in 1 ps. Thus, although the His, heme group geometry is oscillating around an average value at the end of the simulation, there appears to be a longer relaxation process that is not sampled on the time scale of the simulation; e.g., the system may be trapped in a local minimum. Such a convergence to a plateau value is analogous to the behavior found in the simulation of other properties, such as the time correlation functions of interest for the analysis of NMR or fluorescence depolarization measurements (Brooks et al., 1988).

The time evolution of the Fe displacement, relative to the heme, in one of the Mb + CO simulations is presented in Figure 2. The distance used is that between the Fe and the Np plane (plane 1), so that the effect shown is independent of doming. Several stages in the motion of the Fe atom are clearly visible. Initially, the iron atom undergoes a smooth out-of-plane displacement with a time constant of about 50 fs (Figure 2A); the two other simulations have time constants of 30 and 40 fs. Both the spatial range and time scale of this motion are similar to the results obtained for the HI + CO model system (Figure 1A), which indicates that the motions on this time scale are decoupled from the protein. The previous simulation of the photodissociation of an isolated α subunit of HbCO (Henry et al., 1985) found that the inital Fe out-of-plane displacement occurred in 50–150 fs (i.e., as for protoheme). At 0.1 ps, the value of the Fe, Np plane displacement in the present simulation reaches a maximum of about 0.5 Å, essentially the same value as that of the HI + CO system at this time. However, the average distance from the Np plane over the first 0.5 ps is 0.34–0.36 Å in Mb + CO versus an average of 0.47 Å in the HI + CO trajectories. As can be seen in Figures 1A and 2A, there are oscillations in the Fe–Np distance over this time scale; one with a 0.2-ps period corresponds to a libration of the His plane about an axis perpendicular to the heme plane.

Over longer times the Fe···Np distance exhibits a complex evolution. The overall trend of the average iron out-of-plane displacement is an increase with time. However, the distance exhibits several periods in which it increases followed by periods of stabilization or transient decrease. The exact times of the individual relaxation process vary among the three simulations. In all three simulations, processes in the time ranges of 1–4, 10–30, and 60–70 ps occur; the behavior of one simulation is shown in Figure 2, panels B and C. The final values of the Fe···Np distance found in the simulations (taken as averages over the 70–100-ps interval) were between 0.41 and 0.44 Å, which is 0.05–0.1 Å smaller than that found in the HICO system. In all three trajectories, the distance Fe···plane 2 (i.e., the distance of Fe relative to the 24 heavy atoms of the heme porphyrin skeleton) follows the evolution of the Fe···Np plane distance, the former being 40–50% larger than the latter. Thus, the heme doming itself evolves from 0.10–0.11 Å in the first 0.5 ps to 0.17–0.20 Å in the final 30 ps. The final Fe···plane 2 displacement is 0.58–0.64 Å, which is about 0.05–0.1 Å smaller than that found in the HI + CO model system. In the latter part of the trajectory (70–100 ps), the rms fluctuations in the Fe···Np plane distance are 0.05–0.06 Å while the overall Fe rms fluctuations are equal to 0.6 Å; the Fe rms fluctuations in myoglobin at room temperature estimated from Mössbauer and X-ray data are about 0.5 Å (Parak et al., 1987).

The evolution of the Fe distance from heme plane 1 (Figure 2) suggests that structural changes of the heme environment occur in the neighborhood of 50 fs and on time scales in the 1-ps and 10-ps range. The first time constant is associated with the initial Fe atom out-of-plane relaxation, and the three others involve reorganization of the protein. The faster change is primarily an adjustment of the F helix, and the slower processes include more general changes in the protein structure; details will be given elsewhere. It is of interest that the slower time constants are similar to the vibrational relaxation times calculated in the simulation of Henry et al. (1986) and inferred from the measurements of Petrich et al. (1987). Nothing can be said about the very long relaxation (time constant > 100 ps) that leads to the fully relaxed unligated structure. Although the initial heme relaxation may be approximately described as an exponential decay with a 50-fs time constant, the slower processes are more complex in character. Their time scales provide information about the temporal occurrence of consecutive phases of the evolution of the Fe atom out-of-plane displacement that are coupled to protein relaxation. The increasing time scales of the various phenomena correspond to nonexponential behavior, in accord with the analysis of Ansari et al. (1985, 1987).

(B) Time-Resolved Absorption Measurements: Interpretation of Geminate Recombination Data

The results of the time-resolved absorption measurements

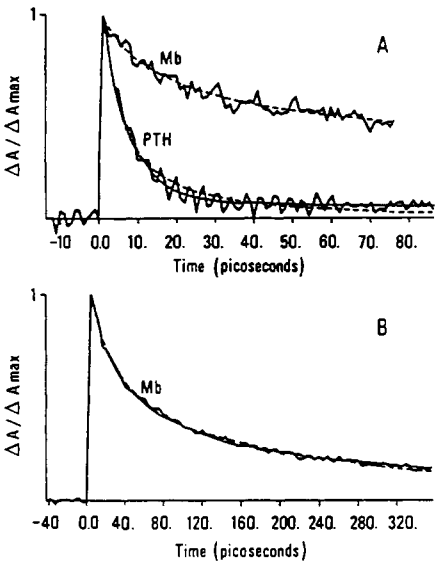

FIGURE 3: (A) Induced absorption at room temperature in PTH NO in 95/5 ethylene glycol/H_2O. λ_{pump} = 580 nm, λ_{probe} = 425 nm. The recombination of NO with PTH was best described by (—): $\Delta A(t)$ = 0.92 exp($-t$/7.0 ps) + 0.08. The 8% of the NO that has not recovered on the 100-ps time scale is due to NO that has escaped from its solvent cage. The best fit to the PTH data with a power law is given by (---): $\Delta A(t) = (1 + t/7.0\text{ ps})^{-1.3}$. As can be seen, the power law fails to fit the long time behavior of the curve. ΔA_{max} = 0.069. The MbNO recombination is also displayed on this time scale. (B) Induced absorption in sperm whale MbNO (100 mM phosphate buffer, pH 7). (—) Power law; (---) double exponential; the two curves cannot be distinguished. The parameters obtained from the fits are given in Table IV. λ_{pump} = 574 nm, λ_{probe} = 438 nm. ΔA_{max} = 0.32.

Table IV: Kinetics of Room Temperature Geminate Rebinding of NO

	power law[a]			double exponential[b]		
heme protein	τ_0 (ps)	n	k^{peak} (ps^{-1})	A	τ_1 (ps)	τ_2 (ps)
HbNO	16.8	1.6	0.10	0.77	10.1	66.7
$\alpha_2^{NO}\beta_2^{+CN}$	15.4	1.5	0.10	0.79	10.3	75.2
$\alpha_2^{+CN}\beta_2^{NO}$	3.7	0.6	0.16	0.76	8.8	202.0
HbNO + IHP	5.4	0.4	0.07	0.54	11.8	250.6
$\alpha_2^{NO}\beta_2^{+CN}$ + IHP	6.9	0.5	0.07	0.56	12.9	264.6
$\alpha_2^{+CN}\beta_2^{NO}$ + IHP	4.4	0.6	0.14	0.74	10.1	222.7
MbNO[c]	32.8	0.7	0.02	0.52	27.6	279.3
LbNO[c]	31.0	0.6	0.02	0.41	12.8	181.0

[a] τ_0 and n are defined in eq 3. $k^{peak} = n/\tau_0$. The values of the parameters are certain to approximately 10%. [b] The parameters are defined in eq 2. The prefactors are normalized so that their sum is unity. [c] Soybean leghemoglobin–NO. Sperm whale myoglobin–NO.

for the various systems studied are shown in Figures 3, 5, and 7. Fits to the data using the functions given in eqs 1–4 are also shown in these figures. The parameters obtained from power law and double-exponential fits are given in Table IV; the parameters from the time-dependent barrier are listed in Table V.

For these systems, eq 3 or 4 (with eqs 10 and 11) provides a satisfactory description of the data. This was determined by visual inspection and by χ^2 and statistical runs tests (Cross & Fleming, 1984). Although the signal-to-noise ratio of the absorption data is good, it still does not allow an unambiguous differentiation between a power law, a time-dependent barrier, or a double exponential.

The room temperature recombination of NO with PTH is contrasted with that of Mb in Figure 3. The PTH kinetics can be fit very well to a single exponential of 7 ps with a small constant base line (eq 1). Because the amplitude of the base line varies with the solvent composition, between 8% for ethylene glycol/water (95/5) and 15% for glycerol/water (67/33) (Petrich and Martin, unpublished results), and because the "base line" shows no recovery in several hundred picoseconds, we conclude that it corresponds to the NO molecules that have escaped from the solvent cage.

In the remainder of the experimental analysis, we consider the appropriateness of describing the kinetics by a distribution of barriers or by a time-dependent barrier.

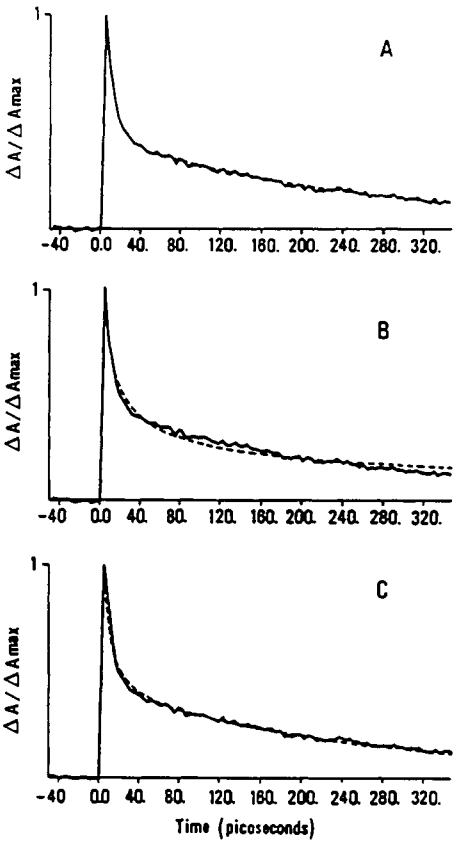

FIGURE 4: Simulations of geminate recombination data. (A) Simulation of a double-exponential absorption recovery to which Gaussian noise is added. The input parameters are such that $\Delta A(t)$ = 0.50 exp($-t$/10.0 ps) + 0.50 exp($-t$/300.0 ps). A fit to a double exponential yield $\Delta_A(t)$ = 0.57 exp($-t$/8.6 ps) + 0.43 exp($-t$/272.5 ps). The agreement between the recovered and input parameters is between 10 and 15% and is as good as can be expected considering the signal-to-noise ratio of the simulated data. (B) The simulated double-exponential recovery of part A fit to a power law. The power law yields $\Delta A(t) = (1 + t/4.6\text{ ps})^{-0.4}$. (C) The simulated double-exponential absorption recovery of part A fit to a function describing a time-dependent barrier (eq 4). Equation 4 yields E_0 = 6.4 × 10^{-3} cal/mol, E_{eq} = 1.8 kcal/mol, A = 7.9 × 10^{10} s^{-1}, and k_{bar} = 3.7 × 10^{10} s^{-1}.

Table V: Parameters Obtained from Fits to a Time-Dependent Barrier[a]

heme protein	E_0[b]	E_{eq}[b]	A[c]	k_{bar}[c]	τ_1^0 (ps)[d]	τ_2^{eq} (ps)[d]
MbNO	0.027	1.2	2.5	1.5	41.9	299.5
HbNO	0.00067	1.5	8.6	1.5	11.6	145.0
HbNO + IHP	0.042	1.8	6.2	2.5	17.3	330.4

[a] E_0 and E_{eq} are the barrier heights determined by the initial Fe–heme plane distance and the "equilibrium" (long time) Fe–heme plane distance, respectively. A is an Arrhenius prefactor. k_{bar} is a time constant that determines the temporal evolution of the barrier height. See eqs 4, 10, and 11. [b] In kcal/mol. [c] In 10^{10} s^{-1}. [d] τ_1^0 is the time constant obtained from $1/k(t)$ in the limit that $t = 0$. Similarly t_2^{eq} is the time constant obtained in the limit that $t \rightarrow \infty$. See eqs 10 and 11. τ_1^0 and τ_2^{eq} are similar to the values of τ_1 and τ_2 compiled for the double-exponential fit in Table IV. Thus, the success of the double-exponential fit may be a result of the limiting behavior of the time-dependent barrier.

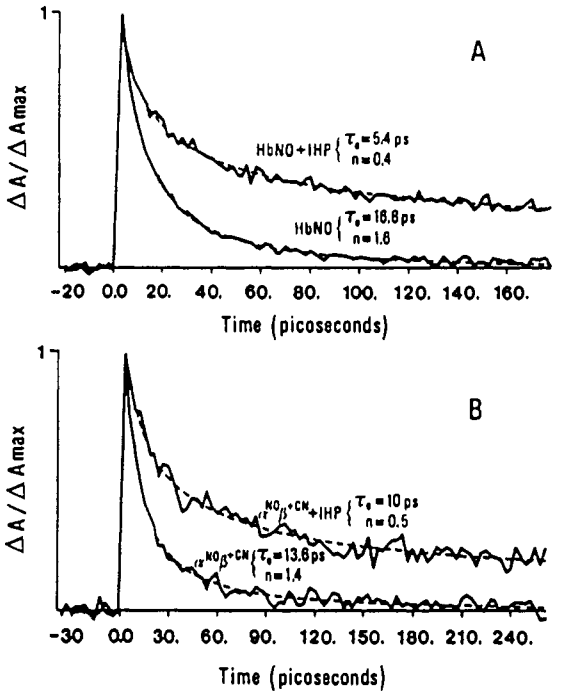

FIGURE 5: Induced absorption at room temperature in Hb (A) and cyanomet valency hybrid Hb (B) in the absence (lower curves) and the presence (upper curves) of 1 mM IHP at pH 6. The dashed lines are fits to a power law. The results of fits to the power law and to a double exponential are given in Table IV. λ_{pump} = 580 nm, λ_{probe} = 438 nm. ΔA_{max}(Hb) = 0.19; ΔA_{max}(Hb+IHP) = 0.18; ΔA_{max}($\alpha_2^{NO}\beta_2^{+CN}$) = 0.12; ΔA_{max}($\alpha_2^{NO}\beta_2^{+CN}$+IHP) = 0.12.

(*i*) *Equilibrium Distributions of Energy Barriers to Geminate Rebinding.* A distribution of energy barriers to rebinding can be calculated from eq 7, which relates the rebinding kinetics to the distribution by a Laplace transform. A simple formula that gives an analytical expression (eq 8) for the distribution function corresponds to the power law (Abramowitz & Stegun, 1970). In this section, we discuss the binding kinetics of heme proteins in terms of distributions that have been calculated from the parameters obtained from fits to a power law. The power law description to obtain the distributions, $g[E(k)]$, is used for its mathematical convenience; it does not imply that the power law is the only way to represent the NO rebinding.

To extract information concerning the degree of nonexponentiality in the ligand binding, we assume that the energy barriers are distributed continuously and that we have a model for the kinetics (eqs 3 and 5). Plots of $g[E(k)]$ versus $E(k)$ can then be used to compare the normalized full widths at half-maxima of the distributions for the various proteins. It is useful to normalize the width to the peak energy of the distribution, $E(k^{peak})$, to be able to compare the degree of nonexponentiality of different proteins because the nonexponentiality depends not on the magnitudes of the barriers but on their "number".

A problem in this procedure is that we do not have ligand binding data as a function of temperature. Thus, we do not know the distribution of Arrhenius prefactors, A, for a given protein or how these prefactors vary among the proteins. It is better, therefore, to plot $g[E(k)]$ against the experimental quantity $-RT \ln k$. In so doing, the data can be examined without making assumptions about the Arrhenius prefactors. Such plots are presented in Figure 6 for MbNO, LbNO, HbNO, and HbNO in the presence of IHP.

An alternative analysis of the data could be carried out by studying distributions of rates, which are model independent,

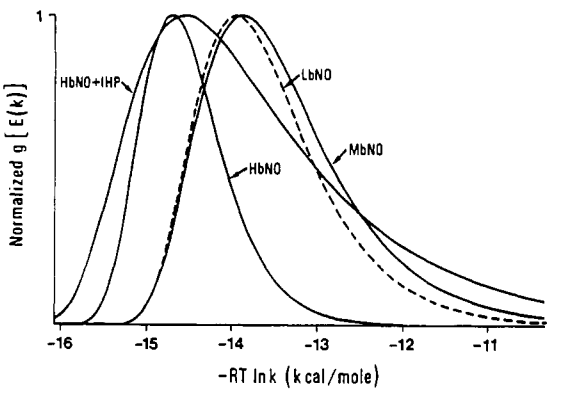

FIGURE 6: Distributions of barriers to ligand rebinding, $g[E(k)]$, for the room temperature geminate recombination of NO with various heme proteins. The figure presents the distributions plotted against $-RT \ln k$. All the distributions are scaled such that their maximum value is unity. See text for a discussion.

instead of energies. Such a possibility was suggested by Austin et al. (1975, see footnote 7). It has been noted that such an analysis can produce unphysical behavior if the exponent n obtained in the fit to the power law (eq 3) is less than or equal to 1 (D. Lambright, S. Balasubramanian, and S. G. Boxer, personal communication).

(*ii*) *Time-Dependent Barrier.* The data for MbNO and HbNO were fit to eqs 4 and 11 according to the following procedure. The complicated nature of this function, a three-tiered exponential, required initially fixing two parameters, k_{bar} and E_{eq}, and minimizing χ^2 by varying A and E_0. The values k_{bar} and E_{eq} were then iteratively varied until an acceptable fit was obtained. We considered values of k_{bar} between 50 and 150 ps. Time constants in this range are in qualitative agreement with the value obtained in the simulation of MbCO dissociation described above. Initial values of E_{eq} were suggested by the data of Doetschman and Utterback (1981) on HbNO crystal and were typically on the order of 1 kcal/mol. This value is consistent with the recent results of Linhares et al. (1990) for nitrosylhemoglobin at low temperature.

The results of using eq 4 to fit the recombination data of MbNO, HbNO, and HbNO + IHP are given in Table V and displayed in Figure 7. As can be seen, eq 4 fits the data very well. This success rationalizes the ability of a sum of two exponentials to fit the data as well as it does; i.e., the two-exponential model is a simplified approximation to a temporally distributed barrier to rebinding. For MbNO (Figure 7A), the values of $k(t)$ in the limits of $t = 0$ and $t \rightarrow \infty$ yield the two time constants 41.9 and 299.5 ps, respectively. These are close to, but not identical with, the values obtained by fitting the MbNO data to two exponentials [27.6 and 279.3 ps (Table IV)]. The same trend is seen in the HbNO kinetics. We note that a simulated recombination trace with equal amounts of 10- and 300-ps exponential components cannot be well fitted by eq 4 (see Figure 4C). Thus, the time-dependent barrier will not fit an arbitrary function.

Discussion

We consider several questions raised by the experiments that demonstrate that NO rebinding is fast and nonexponential at room temperature. The origin of the nonexponential kinetics has a phenomenological aspect (the choice among the different kinetic expressions given in eqs 1–4) and a physical aspect (the significance of the different models). Given the possible models, it is of interest to examine the structural origins of the nonexponential behavior, the differences between the

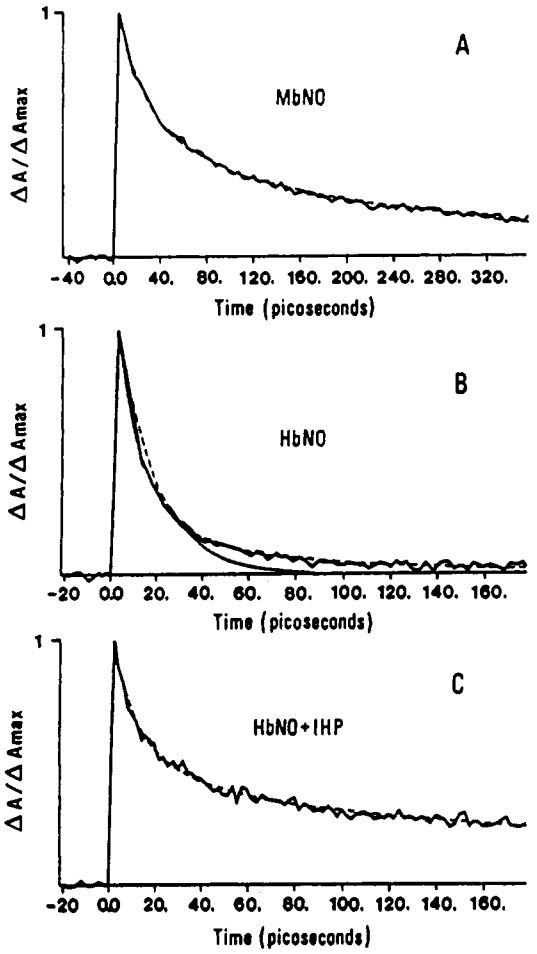

FIGURE 7: Use of a time-dependent barrier (eq 8) to fit the absorption recovery of NO with Mb (A), Hb (B), and Hb + IHP (C). For Hb, also shown is the failure of the best fit single exponential of time constant 17.4 ps to describe the data. The parameters of the time-dependent barrier fits are given in Table V.

various systems studied, and the insights concerning these provided by the molecular dynamics simulations.

(A) Choice of Models. In the analyses of the experimental data, we discussed the appropriateness of the power law (eq 3) and the time-dependent barrier (eq 4) as opposed to a sum of two exponentials (eqs 1 and 2) in describing the rebinding kinetics. While the sum of two exponentials does provide a satisfactory fit to the data, there are a number of reasons why it is physically more reasonable to consider a distribution of barriers to ligand rebinding and hence to apply either eq 3 or eq 4. We discuss the question of equilibrium versus nonequilibrium effects in a subsequent section.

For complex systems, whether biopolymers or other amorphous materials, a range of relaxation times and structural inhomogeneities are found that correspond to strongly nonexponential kinetics for many phenomena at the appropriate temperatures (Bai & Fayer, 1989). Thus, it would be *surprising* if there were not a distribution of rebinding processes. In addition to the studies of Frauenfelder and co-workers, it has been shown that at cryogenic temperatures the electron transfer between the special pair bacteriochlorophyll dimer and the ubiquinone acceptor in photosynthetic bacteria could be modeled by a distribution of donor–acceptor electron-transfer distances (Kleinfeld et al., 1984). Champion and co-workers have interpreted the inhomogeneous broadening in the optical spectra of Mb and MbCO in terms of disorder in the heme–Fe coordinate (Srajer et al., 1986). Furthermore, the nanosecond and subnanosecond fluorescence lifetime data for tryptophan residues in proteins at ambient temperatures can be fitted to distributions of lifetimes (Tanaka & Mataga, 1987; Alcala et al., 1987; Lakowicz et al., 1987; James & Weber, 1985; Siemiaruk & Ware, 1987; Livesey & Brochon, 1987).

It may be argued that since the power law was chosen to fit low-temperature CO rebinding data for Mb over several decades of time because six or seven exponentials were not sufficient (Austin et al., 1975), the power law will fit an arbitrary sum of exponentials. This is incorrect, as shown in Figure 4. We use the simulated data considered in the time-dependent barrier case and show that a recombination trace with equal amounts of 10- and 300-ps exponential components cannot be fit adequately with the power law (Figure 4B). The reason for this is that the parameters n and τ_0 which characterize the power law define a certain distribution of barriers or rates. If the rebinding kinetics contain significant contributions of rate constants that fall outside of this distribution, the power law does not provide an adequate description of the kinetics. The PTH NO recombination is another instance where the power law fails (Figure 3A). A power law with a base-line correction does give an adequate fit, but a single exponential with a base-line correction works as well.

(B) Other Studies of NO Rebinding. Other workers have used picosecond absorption spectroscopy to study NO recombination in heme proteins. Hochstrasser and co-workers (Cornelius et al., 1983) investigated the recombination of NO with normal human Hb. They fit their data to two exponentials with time constants of about 17 and 100 ps. This result is in qualitative agreement with our fit of a double exponential to the HbNO kinetics (Table IV). Their data, however, consist of only nine points over a full-scale time delay of 90 ps, which is not sufficient for a discrimination among different functional forms.

Magde and co-workers (Jongeward et al., 1988, 1986) studied the recombination of NO in Mb. For sperm whale and elephant Mb they report double- and single-exponential recovery kinetics, respectively. In the context of existing X-ray structures (Kuriyan et al., 1986; Ringe et al., 1984) and Raman data, others (Campbell et al., 1987a,b) have interpreted these conclusions in terms of two distal histidine conformations controlling the motion of the ligand in sperm whale Mb. In the case of elephant Mb, where the distal histidine is substituted with glutamine, one might expect only one distal conformation. This could be consistent with the claim of single-exponential recombination behavior.

Although Figures 3 and 4 of Magde and co-workers (Jongeward et al., 1986) do indicate a marked difference in the kinetics of sperm whale and elephant Mb recombination, they do not provide convincing evidence that the recombination is described by a double and a single exponential, respectively. For example, the result cited for elephant Mb is a single exponential with relaxation time $\tau = 1$ ps. The absorption change at 40 ps, however, is still 20% of its initial value. Since the data are not extended beyond 40 ps, it is not clear if the base line that is tacitly included in their fit is really constant (reflecting ligand escape from the heme pocket) or if it decays on a slightly longer time scale. Also, caution must be exercised when comparing data from different species. The substitution of the distal histidine (E7) by glutamine is not the only difference between sperm whale and elephant Mb; there are 28 amino acid differences between two sequences (Dayhoff, 1978; Dene et al., 1980). A recent NMR study by LaMar and co-workers (Lipiny et al., 1990) has shown there are many

differences between the heme pockets of elephant and sperm whale Mb. This indicates that it is important to study the effects of single mutations in a protein (Lambright et al., 1989). In a forthcoming publication, we shall discuss the effect on NO recombination of engineered mutants of human Mb.

(C) Origin of Nonexponential Rebinding: Distributions and/or Relaxation. The role of substates as the source of the nonexponential rebinding kinetics of CO observed in low-temperature Mb has been stressed by Frauenfelder and his co-workers (Austin et al., 1975; Ansari et al., 1985). As mentioned in the introduction, there are two limiting possibilities. In one limit, many protein substates with different barrier heights exist at equilibrium and it is the substate interconversion rate versus the rebinding rate that determines whether or not exponential behavior is observed. In the other limit, the barrier and binding rate are altered by protein relaxation from the ligated to the unligated structure after dissociation so that the relative rate of relaxation and rebinding determines whether the latter shows nonexponential kinetics. The two possible sources of nonexponential behavior are not mutually exclusive and are likely to play a greater or lesser role, depending on the nature of the ligand, the protein, and the temperature, as well as other conditions specifying the system.

The present molecular dynamics simulation results and experimental measurements demonstrate that at room temperature the time scale of the relaxation of photodissociated myoglobin to the equilibrium deoxy structure (on the order of 100 ps) is the same as that of the NO rebinding. For this case nonequilibrium effects are likely to make a significant contribution to the nonexponential behavior. For CO at room temperature, because of the large electronic barrier to ligand binding presented by CO, one does not even begin to observe CO recombination until about 100 ns subsequent to photodissociation (Henry et al., 1983). Thus, myoglobin would be completely relaxed by the time rebinding occurs, and exponential behavior would be expected and is observed.

An analysis of the Mb potential energy surface (Elber & Karplus, 1987) based on a room temperature 300-ps molecular dynamics trajectory (Levy et al., 1985) demonstrated that multiple minima (substates) exist on the accessible potential surface and that the rate of interconversion between them varies from 0.1 to about 150 ps or more. The short-time transitions correspond to similar structures with small conformational changes localized in loops (overall rms differences of about 0.2 Å), while the longer time transitions involved structural changes distributed over the entire protein with rms differences on the order of 2 Å. This result shows that the substate transitions are on the same time scale as the protein relaxation, as might be expected if they cover the same conformational space. In fact, the rms difference between MbCO and Mb in crystal structures is 0.3 Å for the main chain and 0.7 Å for all non-hydrogen atoms, considerably smaller than the conformational space explored by the single Mb simulation at room temperature. A corresponding conclusion has been reached by Parak et al. (1987) on the basis of X-ray temperature factor measurements. Since NO geminate recombination is on the same time scale as the equilibrium fluctuations and nonequilibrium relaxation at room temperature, both processes could contribute to nonexponential rebinding.

At low temperatures, both the rebinding and the protein structural transitions become much slower. Simulations at 80 K (Kuczera et al., 1990) and incoherent neutron scattering experiments (Doster et al., 1989; Smith et al., 1990) indicate that protein fluctuations are relatively harmonic and correspond to oscillations in a single well or substate. This would suggest that the inhomogeneous mechanism of Austin et al. (1975) is dominant at room temperature. A dissociation simulation at 10 K (K. Kuczera and M. Karplus, unpublished results) demonstrates that the initial motion of the iron out of the heme plane still occurs rapidly (40 fs) but that the successive steps involving protein relaxation are much slower. Thus, it is possible that even at low temperatures there is a relaxation contribution to the nonexponential behavior. To examine over what time scale (and for what temperatures) a time-dependent barrier can fit geminate recombination data, we attempted to fit the geminate recombination data of Austin et al. (1975; their Figures 2a and 14) for MbCO in glycerol/H_2O at 120 K to the time-dependent barrier expression in eqs 4 and 11. The time-dependent barrier with parameters $E_0 = 0.8$ kcal/mol, $E_{eq} = 2.6$ kcal/mol, $A = 10^8$ s^{-1}, and $k_{bar} = 2500$ s^{-1} describes the data relatively well up to about 10^{-2} s. The failure of the simple expression to describe the MbCO data after this point should not, however, be interpreted as an invalidation of the time-dependent barrier model. At low temperatures, eq 11 is expected to be replaced by a more complex expression with multiple relaxation times (Bai & Fayer, 1989). This could lead to nonexponential behavior over a much longer time scale. Most likely, the observed kinetics are due to both relaxation and to an inhomogeneous protein population (substates) with different average structures and different relaxation behavior. A detailed analysis of the recombination kinetics of CO in Mb and certain markers for conformational change (Steinbach et al., 1991) provides estimates of the relative contributions of substates and relaxation to the observed nonexponential rebinding as a function of temperature.

(D) Structural Basis of Nonexponential Binding. The difference in NO rebinding kinetics between PTH and Mb demonstrates that the protein plays a significant role. Since the Mb recombination kinetics are nonexponential whereas the PTH kinetics are exponential, a distribution of protein conformations, time independent or time dependent, is implicated in the geminate rebinding of NO to Mb. Further, the rebinding for PTH is considerably faster than that for Mb. Whether the latter is due to a cage effect or involves four-coordinate hemes is not clear.

To try to localize the structural elements controlling the kinetics, we examine the NO results obtained with different heme proteins (see section B under Results). Leghemoglobin (Lb), a monomeric protein, has a significantly larger heme pocket than Mb (Arutyunyan, 1981; Stetskowski, 1983). Its rebinding with NO is nevertheless similar to that of Mb (Table IV). In particular, the $g[E(k)]$ for LbNO and MbNO are very similar. This suggests, in accord with earlier analyses [e.g., Srajer et al. (1988)], that the proximal heme environment is more important than the distal (pocket) region for geminate recombination; for escape from the protein, the distal region plays the dominant role (Elber & Karplus, 1990). It is of interest to note, however, that, for CO rebinding at low temperature, Lb and Mb behave differently.

Hb is a system in which the influence of the proximal environment and the effect of its modification may be examined. A well-defined pathway by which the perturbation of ligation or deligation of the heme in one subunit can be transmitted to the heme in an adjacent subunit has been proposed (Gelin & Karplus, 1977; Gelin et al., 1983). The pathway involves the allosteric core, which consists of the heme, the proximal histidine (HisF8), the F helix, and the FG corner which is in contact with the $\alpha_1\beta_2$ interface. The response of this proximal

heme environment to ligand dissociation and rebinding is thus expected to be significantly different in Mb and Hb. The best evidence comes from a study of the stretching frequency of the Fe–NE2 (HisF8) mode in photodissociated MbCO and HbCO. The frequency of this mode is the same at 30 ps in the MbCO photoproducts as in equilibrium unligated Mb (Findsen et al., 1985a). In the HbCO photoproduct, by contrast, the frequency of the mode does not begin to change for several nanoseconds (Findsen et al., 1985b; Scott & Friedman, 1984; Shelnutt et al., 1979). Further, Friedman et al. (1985) have correlated the frequency of the Fe–His mode with the yield of O_2 geminate recombination in Hb and suggested that the degree of relaxation of the proximal side controls the reactivity of the protein. Also, they measured the 760-nm absorption band of Mb at cryogenic temperatures. This band (Campbell et al., 1987) is not present in the ligated protein and behaves similarly to the Fe–His stretching frequency (Sassaroli & Rousseau, 1987). Because they observed changes in the 760-nm band after a fraction of the dissociated CO molecules had recombined, they associated part of the inhomogeneous width of the band to a distribution of protein conformations correlated with the Fe–His mode. A more detailed analysis of this band has been made recently (Frauenfelder et al., private communication).

The absorption data at room temperature show that NO rebinding in Hb (Figure 7) is faster than in Mb. In terms of the time-dependent barrier model, this is consistent with an unrelaxed or partly relaxed Hb molecule. Evidence for the structural origin of this difference is obtained from NO rebinding to Hb in the presence of the allosteric effector, inositol hexaphosphate (IHP), at acid pH. After photodissociation (Figure 5 and Table IV), NO rebinding to the α subunits of $\alpha_2\beta_2^{+CN}$ of Hb is much slower in the presence of IHP than in its absence. Also, the addition of IHP to HbNO broadens $g[E(k)]$ by about a factor of 2. The effect on the β hemes in the $\alpha_2^{+CN}\beta_2$ hybrid is much smaller (Table IV). IHP binds in the central cavity between the amino termini of the β chains approximately 34 Å from the ligand binding site in the α subunits (Arnone & Perutz, 1974; Szabo & Perutz, 1976). The bond between the Fe and the proximal histidine is cleaved or considerably weakened in the α subunits of HbNO upon binding of IHP (Perutz et al., 1976; Maxwell & Caughey, 1976). The α heme is essentially planar because the NO ligand opposes the out-of-plane motion of the Fe, even though IHP imposes a T-quaternary structure on the molecule at acidic pH (Perutz et al., 1976).

The slower rebinding of NO to Hb with IHP can be interpreted as resulting from the rapid formation of the bond between Fe and the NE2 of the proximal histidine after dissociation of the ligand as the heme is no longer constrained to be planar. The time for the rebinding of the Fe to the proximal His is estimated to be less than 300 fs; the upper limit of 300 fs is the time constant for the appearance of the unligated ground-state species (Martin et al., 1983; Petrich et al., 1988a). Since the protein is expected to have a conformation close to the unligated state in the absence of an Fe–His bond, a large barrier to rebinding results from the Fe–His bond formation. This contrasts with the expectation for rebinding without prior Fe–His bond formation; the four-coordinate heme would produce single-exponential recombination that is more rapid than that observed in HbNO in the absence of IHP; in fact, results similar to those for PTH (Figure 3) would be expected. Figure 5 illustrates the retardation in the rebinding. The change in the NO recombination kinetics in the presence of IHP supports the importance of interactions on the proximal side of the heme in the geminate reginding of NO.

The difference in structure and reactivity between the α and β chains constitutes an intrinsic heterogeneity in Hb (Perutz et al., 1976; Maxwell & Caughey, 1976; Ogata & McConnell, 1972; Banerjee et al., 1973; Edelstein, 1974; Szabo & Karplus, 1975; Inubushi et al., 1986). The NO rebinding in $\alpha_2^{NO}\beta_2^{+CN}$ (Figure 5B and Table IV) indicates that the α subunits comprise the most significant part of the kinetics observed in Hb (Figure 5A). Thus, the behavior of the cyanomet valency hybrids of Hb (Figure 5B and Table IV) confirms that the nonexponential rebinding occurs in a particular subunit, rather than being the result of the superposition of the α and β kinetics.

The simulations of Mb have shown that at equilibrium after photodissociation the Fe–Np plane distance fluctuates by 0.05–0.06 Å. This value corresponds to the estimate of Srajer et al. (1988) for the distance fluctuation required to obtain the observed barrier distribution in their phenomenological model for nonexponential binding. However, in the simulations the Fe–Np plane distance continues to increase by an additional 0.1–0.15 Å on a 1–100-ps time scale, following the initial rapid (50-fs) out-of-plane motion of the heme iron. Thus, as already discussed, the Fe motion relative to the heme due to protein relaxation after photodissociation may give rise to a time-dependent barrier that results in nonexponential recombination kinetics. Even in the limit of an ensemble of conformationally identical proteins the structural relaxation of the protein triggered by ligand dissociation can produce nonexponential binding. In this case, the ligand would encounter an effective distribution of barriers because the barrier in each protein is evolving on the time scale of the recombination. Since the time scale of the Fe–heme plane relaxation (Figure 2C) corresponds to the time in which a significant portion of NO molecules have been shown to recombine (Figures 3 and 5), it is plausible to consider the Fe–heme plane distance relaxation as a possible source of the observed nonexponential rebinding.

If the Fe–heme plane coordinate is most important in determining the rate of geminate ligand rebinding, the more the Fe is out of plane, the greater will be the barrier to ligand rebinding. This is the result of fitting the data (Figure 7) to eq 4. Namely, at early times, the barrier is low and $k(t\rightarrow 0)$ is large because the iron is nearer its in-plane configuration; at longer times $k(t\rightarrow\infty)$ is smaller because the out-of-plane displacement of the iron atom presents an increasing barrier to rebinding. The ability of a double exponential decay to describe the data may be due to the limiting behavior of $k(t)$ rather than to two discrete barriers as has been proposed (Jongeward et al., 1988).

Conclusions

NO rebinding had been used to examine the factors that influence geminate recombination on a picosecond time scale at room temperature. Since the rebinding is found to be nonexponential from time-resolved absorption experiments, a distributed barrier model is used to describe the kinetics, though a two-exponential model cannot be excluded.

On the basis of molecular dynamics simulations of Mb and heme–imidazole subsequent to ligand dissociation, it is suggested that the nonexponential behavior can result from two physically different phenomena. There can be a distribution of rates that is due to a range of barriers present in an inhomogeneous protein population (substates) or to relaxation of a protein coordinate following a perturbation such as ligand dissociation. These processes can give rise to a time-inde-

pendent or a time-dependent distribution of activation barriers, both of which can produce a spectrum of rebinding rates. In the latter model, the protein molecules that make up the ensemble may relax with the same time constants. Such relaxation is in accord with the molecular dynamics simulations and can give rise to nonexponential rebinding kinetics. It provides an acceptable fit to the room temperature geminate rebinding data for NO. In the limits of very short and very long times, this kinetic model yields rate constants that correspond to those obtained from a double-exponential fit to the data.

As the effective coordinate involved in the time-dependent barrier, we focus on the Fe–heme distance. It is, in turn, modulated by the protein relaxation. The latter is the major factor that regulates the distribution of geminate rebinding rates over a picosecond time scale at room temperature. Analysis of the change of the Fe–Np plane distance with time in Mb after dissociation shows a series of events in the 50-fs–100-ps time scale. Thus, for NO at room temperature, it is likely that relaxation in the picosecond time scale plays an important role. Indirect evidence for this is provided by a drastic reduction of NO rebinding rate of Hb and cyanomet hybrids when IHP is bound. Since the Fe–proximal histidine bond is known to be weakened in the α subunits in the presence of IHP, this result indicates that, after the NO is dissociated, the Fe–histidine bond is re-formed in less than 300 fs and the proximal environment has a T-like tertiary structure.

It is difficult to separate the source of distributed binding kinetics into contributions from protein molecules that have different conformations (substates) and contributions from the time-dependent evolution of coordinates in individual protein molecules. Depending on the temperature, the ligand, and the protein, the two mechanisms are expected to vary in importance. For NO at room temperature, geminate recombination, transitions between substates, and relaxation after dissociation are all on the 0.1–100-ps time scale. The present simulations, although performed for CO, should be generally applicable to the relaxation of myoglobin at room temperature both after photodissociation and after dissociation without photolysis of other small ligands (e.g., NO and O_2). Although the qualitative aspects of the dynamics are clear from the present analysis and that of Frauenfelder and co-workers (Steinbach et al., 1991), a complete quantitative description at the atomic level will require more experiments and simulations. Simulations for different temperatures, coupled with a detailed model for the ligation step, would aid in our understanding of the reaction.

ACKNOWLEDGMENTS

We thank B. Bohn and F. Stetskowski-Marden for preparation of the samples. We acknowledge helpful conversations with D. Lambright, S. Balasubramanian, and S. G. Boxer of Stanford University concerning the interpretation of the distribution functions. We thank H. Frauenfelder for helpful comments on the manuscript and for providing results prior to publication.

Registry No. HICO, 71802-35-2; HI, 54832-27-8; IHP, 83-86-3; L-His, 71-00-1; Fe, 7439-89-6; nitrosylprotoheme, 54854-55-6.

REFERENCES

Abramowitz, M., & Stegun, I. A. (1970) *Handbook of Mathematical Functions*, Dover, New York.

Agmon, N. (1985) *J. Chem. Phys. 82*, 2056.

Agmon, N., & Hopfield, J. J. (1983) *J. Chem. Phys. 79*, 2042–2053.

Alberding, N., Austin, R. H., Chan, S. S., Eisenstein, L., Frauenfelder, H., Gunsalus, I. C., & Nordlund, T. M. (1976) *J. Chem. Phys. 65*, 4701.

Ansari, A., Berendzen, J., Bowne, S. F., Frauenfelder, H., Iben, J. E. T., Sauke, T. B., Shyamsunder, E., & Young, R. D. (1985) *Proc. Natl. Acad. Sci. U.S.A. 82*, 5000.

Ansari, A., Berendzen, J., Braunstein, D., Cowen, B. R., Frauenfelder, H., Hong, M. K., Iben, I. E. T., Johnson, J. B., Ormos, P., Sauke, T. B., Scholl, R., Schulte, A., Steinbach, P. J., Vittitow, J., & Young, R. D. (1987) *Biophys. Chem. 26*, 337.

Appleby, C. A. (1962) *Biochim. Biophys. Acta 60*, 226.

Arnone, A., & Perutz, M. F. (1974) *Nature (London) 249*, 34.

Arutyunyan, E. G. (1981) *Mol. Biol. (Moscow) 15*, 27.

Austin, R. H., Beeson, K. W., Eisenstein, L., Frauenfelder, H., & Gunsalus, C. (1975) *Biochemistry 14*, 5355.

Bai, Y. S., & Fayer, M. D. (1989) *Phys. Rev. B 39*, 11066.

Baldwin, J. M., & Chothia, C. (1979) *J. Mol. Biol. 129*, 175.

Banerjee, R., Stetzkowski, F., & Henry, Y. (1973) *J. Mol. Biol. 73*, 455.

Bevington, P. R. (1969) *Data Reduction and Error Analysis in the Physical Sciences*, McGraw-Hill, New York.

Brooks, B. R., Bruccoleri, R. E., Olafson, B. D., States, D. J., Swaminathan, S., & Karplus, M. (1983) *J. Comput. Chem. 4*, 187.

Brooks, C. L., III, Karplus, M., & Pettitt, B. M. (1988) *Proteins: A Theoretical Perspective of Dynamics, Structure, and Thermodynamics*, Advances in Chemical Physics 71, John Wiley & Sons, New York.

Campbell, B. F., Chance, M. R., & Friedman, J. M. (1987a) *Science 238*, 373.

Campbell, B. F., Chance, M. R., & Friedman, J. M. (1987b) *J. Biol. Chem. 262*, 14885.

Case, D. A., & Karplus, M. (1979) *J. Mol. Biol. 132*, 343.

Chernoff, D. A., Hochstrasser, R. M., & Steele, W. A. (1980) *Proc. Natl. Acad. Sci. U.S.A. 77*, 5606.

Cornelius, P. A., Hochstrasser, R. M., & Steele, W. A. (1983) *J. Mol. Biol. 163*, 119.

Cross, A. J., & Fleming, G. R. (1984) *Biophys. J. 46*, 45.

Dayhoff, M. O. (1978) *Atlas of Protein Sequence and Structure*, Vol. 5, Suppl. 3, National Biomedical Research Foundation, Silver Springs, MD.

Debrunner, P. G., & Frauenfelder, H. (1982) *Annu. Rev. Phys. Chem. 33*, 283.

Dene, H., Goodman, M., & Romero-Herrera, A. E. (1980) *Proc. R. Soc. London B 207*, 111.

Doetschman, D. C., & Utterback, S. G. (1981) *J. Am. Chem. Soc. 103*, 2847.

Doster, W., Cusack, S., & Petry, W. (1989) *Nature (London) 337*, 754–755.

Edelstein, S. J. (1974) *Biochemistry 13*, 4998.

Elber, R., & Karplus, M. (1987a) *Science 235*, 318.

Elber, R., & Karplus, M. (1987b) *Chem. Phys. Lett. 139*, 375.

Elber, R., & Karplus, M. (1990) *J. Am. Chem. Soc. 112*, 9161.

Findsen, E. W., Scott, T. W., Chance, M. R., Friedman, J. M., & Ondrias, M. R. (1985a) *J. Am. Chem. Soc. 107*, 3355.

Findsen, E. W., Friedman, J. M., Ondrias, M. R., & Simon, S. R. (1985b) *Science 229*, 661.

Frauenfelder, H., & Wolynes, P. G. (1985) *Science 229*, 337.

Frauenfelder, H., Petsko, G. A., & Tsernoglu, D. (1979) *Nature (London) 280*, 558.

Friedman, M., Scott, T. M., Fisanick, G. J., Simon, S. R., Findsen, E. W., Ondrias, M. R., & MacDonald, V. W. (1985) *Science 299*, 187.
Gelin, B. R., & Karplus, M. (1977) *Proc. Natl. Acad. Sci. U.S.A. 74*, 801.
Gelin, B. R., Lee, A. W.-M., & Karplus, M. (1983) *J. Mol. Biol. 171*, 489.
Henry, E. R., Sommer, J. H., Hofrichter, J., & Eaton, W. A. (1983) *J. Mol. Biol. 166*, 443.
Henry, E. R., Levitt, M., & Eaton, W. A. (1984) *Proc. Natl. Acad. Sci. U.S.A. 82*, 2034.
Henry, E. R., Eaton, W. A., & Hochstrasser, R. M. (1986) *Proc. Natl. Acad. Sci. U.S.A. 83*, 8982.
Hofrichter, J., Sommer, J. H., Henry, E. R., Eaton, W. A. (1983) *Proc. Natl. Acad. Sci. U.S.A. 80*, 2235.
Inubushi, T., D'Ambrosio, C., Ikeda-Saito, M., & Yonetani, T. (1986) *J. Am. Chem. Soc. 108*, 3799.
James, D. R., & Ware, W. R. (1985) *Chem. Phys. Lett. 120*, 445.
Janes, S. M., Dalickas, G. A., Eaton, W. A., & Hochstrasser, R. M. (1988) *Biophys. J. 54*, 545.
Jongeward, K. A., Marsters, J. C., & Magde, D. (1986) in *Ultrafast Phenomena V* (Fleming, G. R., & Siegman, A. E., Eds.) p 427, Springer, Berlin.
Jongeward, K. A., Magde, D., Taube, D. J., Marsters, J. C., Traylor, T. G., & Sharma, V. S. (1988) *J. Am. Chem. Soc. 110*, 380.
Keyes, M. H., Falley, M., & Lumry, R. J. (1971) *J. Am. Chem. Soc. 93*, 2035.
Kleinfeld, D., Okamura, M. Y., & Feher, G. (1984) *Biochemistry 23*, 5780.
Korzekwa, K., Trager, W., Gouterman, M., Spangler, D., & Loew, G. H. (1985) *J. Am. Chem. Soc. 107*, 4273.
Kuczera, K., Kuriyan, J., & Karplus, M. (1990) *J. Mol. Biol. 213*, 351–373.
Kuriyan, J., Wilz, S., Karplus, M., & Petsko, G. A. (1986) *J. Mol. Biol. 192*, 133.
Lakowicz, J. R., Cherek, H., Grycaynski, I., Joshi, N., & Johnson, M. L. (1987) *Biophys. Chem. 28*, 35.
Lambright, D., Balasubramanian, S., & Boxer, S. G. (1989) *J. Mol. Biol.* (submitted for publication).
Levy, R. M., Sheridan, R. P., Keepers, J. W., Dubey, G. S., Swaminathan, S., & Karplus, M. (1985) *Biophys. J. 48*, 509.
Linhares, M. P., El-Jaick, L. J., Bemski, G., & Wajnberg, E. (1990) *Int. J. Biol. Macromol. 12*, 59.
Livesey, A. K., & Brochon, J. C. (1987) *Biophys. J. 52*, 693.
Marden, M. C., Hazard, E. S., III, & Gibson, Q. H. (1986) *Biochemistry 25*, 2786.
Martin, J. L., Migus, A., Poyart, C., Lecarpentier, Y., Astier, R., & Antonetti, A. (1983) *Proc. Natl. Acad. Sci. U.S.A. 80*, 173.
Maxwell, J. C., & Caughey, W. C. (1976) *Biochemistry 15*, 388.
Ogata, R. T., & McConnell, H. M. (1972) *Proc. Natl. Acad. Sci. U.S.A. 69*, 335.
Parak, F., Hartmann, H., Aumann, K. D., Reuscher, H., Rennekamp, G., & Bartunik, H. (1987) *Eur. Biophys. J. 15*, 237.
Perutz, M. F., Kilmartin, J. V., Nagai, K., Szabo, A., & Simon, S. R. (1976) *Biochemistry 15*, 378.
Perutz, M. F., Fermi, G., Luisi, B., Shaanan, B., & Liddington, R. C. (1987) *Acc. Chem. Res. 20*, 309.
Petrich, J. W., Martin, J. L., Houde, D., Poyart, C., & Orszag, A. (1987) *Biochemistry 26*, 7914.
Petrich, J. W., Poyart, C., & Martin, J. L. (1988a) *Biochemistry 27*, 4049.
Petrich, J. W., Martin, J. L., & Breton, J. (1988b) in *Ultrafast Phenomena VI* (Yajima, T., et al., Eds.) p 576, Springer, Berlin.
Phillips, D. C. (1978) *Nature (London) 273*, 247.
Phillips, S. E. V. (1980) *J. Mol. Biol. 142*, 531.
Phillips, S. E. V. (1981) *The X-ray Structure of Deoxy-Mb (pH 8.5) at 1.4 Å Resolution*, Brookhaven Protein Data Bank.
Plonka, A. (1988) *Chem. Phys. Lett 151*, 466.
Ringe, D., Petsko, G. A., Kerr, D. E., & Ortiz de Montellano, P. R. (1984) *Biochemistry 23*, 2.
Sassaroli, M., & Rousseau, D. L. (1987) *Biochemistry 23*, 3092.
Scott, T. W., & Friedman, J.-M. (1984) *J. Am. Chem. Soc. 106*, 5677.
Shelnutt, J. A., Rousseau, D. L., Friedman, J.-M., & Simon, S. R. (1979) *Proc. Natl. Acad. Sci. U.S.A. 76*, 4409.
Siemiaruk, A., & Ware, W. R. (1987) *Chem. Phys. Lett 140*, 277.
Smith, J., Kuczera, K., & Karplus, M. (1990) *Proc. Natl. Acad. Sci. U.S.A 87*, 1601.
Srajer, V., Schomacker, K. T., & Champion, P. M. (1986) *Phys. Rev. Lett. 57*, 1267.
Srajer, V., Reinisch, L., & Champion, P. M. (1988) *J. Am. Chem. Soc. 110*, 6656.
Steinbach, P. J., Ansari, A., Berendzen, J., Braunstein, D., Chu, K., Cowen, B. R., Ehrenstein, D., Frauenfelder, H., Johnson, J. B., Lamb, D. C., Luck, S., Mourant, J. R., Neinhaus, G. U., Ormos, P., Philipp, R., Xie, A., & Young, R. D. (1991) *Biochemistry* (following paper in this issue).
Stetzkowski, F. (1983) Thesis, Université de Paris.
Szabo, A. (1978) *Proc. Natl. Acad. Sci. U.S.A. 75*, 2108.
Szabo, A., & Perutz, M. F. (1976) *Biochemistry 15*, 4427.
Takano, T. (1977) *J. Mol. Biol. 110*, 537.
Tanaka, F., & Mataga, N. (1987) *Biophys. J. 51*, 487.
Tentori, L., Vivaldi, G., Carta, S., Marinucci, M., Massa, A., Antonini, E., & Brunori, M. (1971) *FEBS Lett. 12*, 181.
Van Gunsteren, W. V., & Berendsen, H. J. C. (1977) *Mol. Phys. 34*, 311.
Yu, L. P., La Mar, G. N., & Mizukami, H. (1990) *Biochemistry 29*, 2578.